The International Journal of Advanced Manufacturing Technology (2024) 133:1639–1650
https://doi.org/10.1007/s00170-024-13794-3

ORIGINAL ARTICLE

# Influence of tool flank wear considering tool edge radius on instantaneous uncut chip thickness and cutting force in micro-end milling

Shuaishuai Gao[1] · Xianyin Duan[2] · Kunpeng Zhu[3] · Yu Zhang[2]

Received: 12 July 2023 / Accepted: 20 May 2024 / Published online: 3 June 2024


## Abstract

Accurate theoretical analysis and modeling of instantaneous uncut chip thickness (IUCT) play a crucial role in the cutting force prediction of the micro-milling process. Tool wear and tool runout have a significant influence on the IUCT and become key factors to be considered. An IUCT model covering the influence of tool runout and tool flank wear considering tool edge radius is proposed. Based on this the prediction model of the cutting force is constructed in the micro-end milling process. Firstly, an actual tool radius model considering tool flank wear and tool edge radius is analyzed. The IUCT model is established by constructing the trochoidal trajectories of the current cutting edge and all cutting edges in the previous cycle considering tool flank wear and tool runout. Moreover, tool flank wear and tool runout are considered in the determination of cutter-workpiece engagement and the calibration of cutting force coefficients. Effectiveness of the established cutting force model is verified by micro milling experiments and statistical analysis. Results show that tool flank wear has a significant effect on the cutting forces of the three directions, and the influence of tool flank wear on the IUCT is small in a certain range. This work for predicting the IUCT and cutting force sheds new light on revealing various derived physical phenomena such as deformation, heat, and stress in the micro-cutting process.

## Highlights

**The instantaneous uncut chip thickness model covering the influence of tool runout and tool flank wear considering tool edge radius is proposed.**
**The micro-milling cutting force based on instantaneous uncut chip thickness is predicted from the mechanism level.**
**Effectiveness of the established cutting force model is verified by micro-milling experiments and statistic analysis.**
**The influence of tool flank wear on the instantaneous uncut chip thickness and cutting force is analyzed.**

**Keywords** Micro-end milling · Cutting force · Instantaneous uncut chip thickness · Tool flank wear · Tool edge radius · Tool runout

✉ Xianyin Duan
xyduan@wust.edu.cn

✉ Kunpeng Zhu
zhukp@iamt.ac.cn

[1] School of Artificial Intelligence, Jianghan University, Wuhan 430056, China

[2] Key Laboratory of Metallurgical Equipment and Control Technology, Ministry of Education, Wuhan University of Science and Technology, Wuhan 430081, China

[3] Institute of Intelligent Machines, Hefei Institutes of Physical Science, Chinese Academy of Sciences, Hefei 230031, China

## 1 Introduction

The fast-increasing demands for miniature components and products generate a fundamental internal driving force for the development of micro-manufacturing technology in the fields of microelectronics, bioengineering, optics, and aerospace [1–4]. As one of the most productive micro-manufacturing technologies, micro-milling technology plays an important role in manufacturing a variety of complex parts with the advantages of high efficiency, high accuracy, and good flexibility [1–4].

As the force required to remove the material and turn it into the chip, cutting force is the most basic and direct physical phenomenon in the micro-milling process. The research on the accurate prediction of cutting force in the micro-milling process is of great significance to study the cutting mechanism and derived physical phenomena, such as cutting temperature, tool wear, and tool durability, as well as for the study of process optimization, the improvement of machining quality, efficiency, and the stability of the machining process. Accordingly, the modeling of micro-milling force has attracted extensive attention from researchers in the advanced manufacturing field.

The mechanical cutting force model [5] is a well-tested and received method for the prediction of the cutting force. Theoretical analysis and modeling of the instantaneous undeformed chip thickness, namely IUCT, is a crucial part of the mechanical force model. The IUCT is generally analyzed and determined by trochoidal trajectories of cutting edge [6]. Furthermore, the IUCT is also influenced by multiple factors such as tool wear [7, 8], tool runout [9], and minimum uncut chip thickness [10]. Rodríguez et al. [11] also took the tool deflection into account in the modeling of IUCT and the dynamic cutting force equation of the micro-milling process. Zhang et al. [12] proposed a micro-end milling force model considering tool runout with axial and inclined offset and minimum chip thickness. Li et al. [13] built a general IUCT model considering tool runout based on the trochoidal trajectories of cutting edge in a cycle and derived a criterion for judging the single-edge cutting phenomenon in micro milling of multi-teeth. Moges et al. [14] used an iterative algorithm to determine the IUCT considering tool deflection. Wojciechowski et al. [15] researched the chip thickness accumulation effect in micro-milling force model. Wan et al. [16] deeply studied the dead zone effect and material separation phenomenon in the cutting force prediction. Many researchers also attempted to establish a more accurate IUCT model by considering the effects of tool runout, elastic recovery, and minimum cutting thickness by studying the function of all previous tooth trajectories on the current tooth trajectory [17–20]. Wan et al. [21] considered the influence of tool deflection in the trajectories of cutting edges and established the IUCT model by considering the minimum cutting thickness. The previous researches enrich the understanding of element geometry and micro milling mechanism and improve the accuracy of cutting force prediction.

However, due to the rapid improvement of service performance requirements of equipment, more difficult-to-cut materials with higher hardness and strength are selected for micro-parts and products of equipment. The cutting of these difficult-to-cut materials aggravates the wear velocity of micro-milling cutters, making tool wear, especially tool flank wear the main form of wear, a significant factor affecting the accurate prediction of cutting force. According to the summary of existing research literature, some researchers considered the influence of tool flank wear on cutting force in the cutting force coefficients [8, 22–25]. In the actual process, it is important and laborious task to measure the tool edge radius and tool flank wear VB. Zhang et al. [7] measured the tool edge radius by the Scanning Electron Microscope. Li et al. [23] used an industrial digital camera to measure the tool flank wear of the micro-end mill in the bottom face.

Some researchers considered the influence of tool flank wear on cutting force in IUCT but ignored the tool edge radius. In addition, tool runout is also an important factor that cannot be ignored in affecting machining accuracy in the micro-milling process. Therefore, this paper proposes to research the influence of tool flank wear considering tool edge radius on the IUCT in micro-end milling and build the cutting force model covering the influence. In this research, the radius of the worn micro-end mill is first analyzed, in which the tool edge radius is considered. Then the theoretical analysis and modeling of IUCT are described based on the relation between trochoidal trajectories of the current cutting edge and all cutting edges in the previous cycle considering the actual radius of the worn tool and tool run out. On this basis, the cutting force model in the micro-milling process is constructed, in which cutting force coefficients and cutter-workpiece engagement covered the influences of tool flank wear, tool edge radius, and tool runout. Finally, the effectiveness of the proposed model is verified through statistical analysis, and the influence of tool flank wear on IUCT and cutting force is analyzed and discussed. This research can promote the accurate prediction method of cutting force in micro-milling and be used in optimizing process parameters and improving machining accuracy.

## 2 Cutting force modeling

### 2.1 General cutting force model

The geometric relationship of the micro-end milling process is analyzed for the the cutting forces modeling as shown in Fig. 1.

A representative micro-end mill with two teeth is used, and the Cartesian coordinate system *O-xyz* is set up in Fig. 1. The origin *O* of the coordinate system is located at the bottom center of the micro-end mill. The *x*-axis is along the feed direction of the tool, and the *z*-axis is upward along the tool axis. The *y*-axis is determined accordingly, as shown in Fig. 1(b). Based on the mechanical modeling method [5], the cutting edge is divided into several discrete elements along the *z*-axis direction (Fig. 1(b)). The point *P* is an arbitrary fixed point on the *i*th ($i=0, 1, 2, \ldots, N$-1) cutting edge at a specific axial

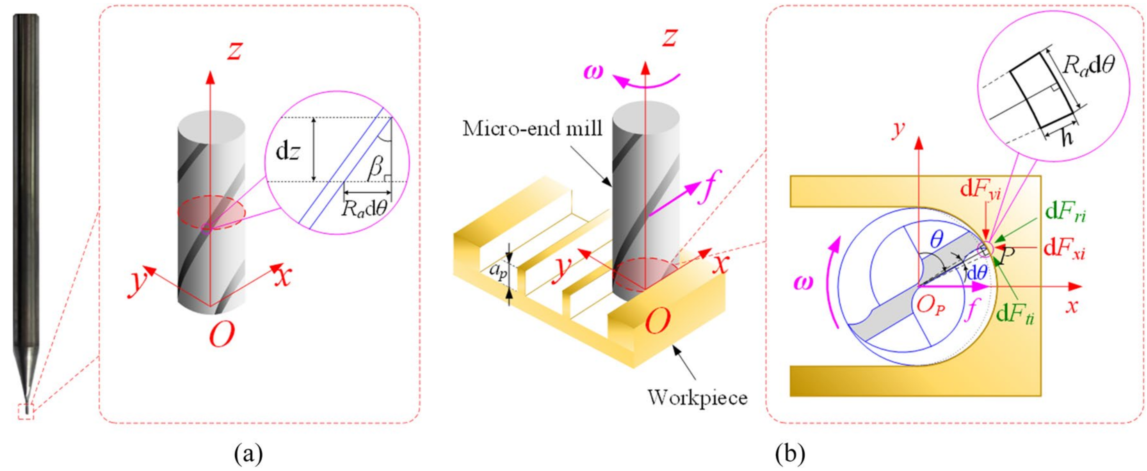


**Fig. 1** Geometrical parameters of the micro-end milling process. (**a**) Micro-end mill; (**b**) the micro-end milling progress and element cutting forces

cutting depth $z$ (μm), where $N$ is the total number of the cutting edges, and the ordinal number $i$ of the cutting edge is set counterclockwise. Accordingly, the tangential cutting force$F_{ti}(\theta)$, radial cutting force$F_{ri}(\theta)$, and axial cutting force $\mathrm{d}F_{ai}(\theta)$ of the element are as follows.

$$\begin{cases} \mathrm{d}F_{ti}(\theta) = K_{tc}h(\theta)\mathrm{d}z, \\ \mathrm{d}F_{ri}(\theta) = K_{rc}h(\theta)\mathrm{d}z, \\ \mathrm{d}F_{ai}(\theta) = K_{ac}h(\theta)\mathrm{d}z, \end{cases} \tag{1}$$

where $K_{tc}$, $K_{rc}$ and $K_{ac}$ are the actual cutting force coefficients in the tangential, radial, and axial directions respectively, $h(\theta)$ is the thickness of the element, i.e., instantaneous uncut chip thickness, $\theta$ is the radial immersion angle of the element, and

$$\theta(i,t,z) = \omega t - \frac{2\pi i}{N} - \frac{z\tan\beta}{R_a} \tag{2}$$

where $R_a$ is the actual radius of the tool, $\beta$ is the helix angle of the tool, $\omega$ is the angular velocity of the spindle(rad/s), and $\omega = \frac{2\pi n}{60}$, $n$ is spindle speed(r/min), $t$ is the time(s). d$z$ is the height of the element as shown in Fig. 1(a), and

$$\mathrm{d}z = \frac{R_a d\theta}{\tan\beta} \tag{3}$$

where $d\theta$ is the length of the element in Fig. 1(b).

According to Fig. 1 (b), the element cutting forces in the $x$-, $y$- and $z$-axis directions are

$$\begin{pmatrix} \mathrm{d}F_{xi}(\theta) \\ \mathrm{d}F_{yi}(\theta) \\ \mathrm{d}F_{zi}(\theta) \end{pmatrix} = \begin{pmatrix} -\cos\theta & -sin\theta & 0 \\ sin\theta & -\cos\theta & 0 \\ 0 & 0 & 1 \end{pmatrix} \begin{pmatrix} \mathrm{d}F_{ti}(\theta) \\ \mathrm{d}F_{ri}(\theta) \\ \mathrm{d}F_{ai}(\theta) \end{pmatrix} \tag{4}$$

Integrate the two sides of the above equations with respect to $\theta$ separately in the cutter-workpiece engagement, and summing up the cutting forces of each flute, we can obtain the total cutting forces at the rotation angle $\varphi$ as

$$\begin{pmatrix} F_x(\varphi) \\ F_y(\varphi) \\ F_z(\varphi) \end{pmatrix} = \frac{R_a}{\tan\beta} \begin{pmatrix} -\sum_{i=0}^{N-1}\int_{\theta_{\mathrm{en}}}^{\theta_{\mathrm{ex}}}\cos\theta h(\theta)d\theta & -\sum_{i=0}^{N-1}\int_{\theta_{\mathrm{en}}}^{\theta_{\mathrm{ex}}}\sin\theta h(\theta)d\theta & 0 \\ \sum_{i=0}^{N-1}\int_{\theta_{\mathrm{en}}}^{\theta_{\mathrm{ex}}}\sin\theta h(\theta)d\theta & -\sum_{i=0}^{N-1}\int_{\theta_{\mathrm{en}}}^{\theta_{\mathrm{ex}}}\cos\theta h(\theta)d\theta & 0 \\ 0 & 0 & \sum_{i=0}^{N-1}\int_{\theta_{\mathrm{en}}}^{\theta_{\mathrm{ex}}}h(\theta)d\theta \end{pmatrix} \begin{pmatrix} K_{tc} \\ K_{rc} \\ K_{ac} \end{pmatrix} \tag{5}$$

where $\varphi = \omega t$, $\theta_{\mathrm{en}}$ and $\theta_{\mathrm{ex}}$ are the entry angle and exit angle respectively, and they are both determined by the cutting edge trochoidal trajectories. Cutting force coefficients $K_{tc}$, $K_{rc}$ and $K_{ac}$ are calibrated by considering tool flank wear and tool runout. The cutting force coefficients are modeled as a quadratic polynomial of the tool flank wear $VB$ respectively. By using the measured cutting forces at different milling stages and Eq. (5) to obtain the inverse solutions, the cutting force coefficients can be fitted by adopting the Least squares method. $h(\theta)$ will be given in the following.

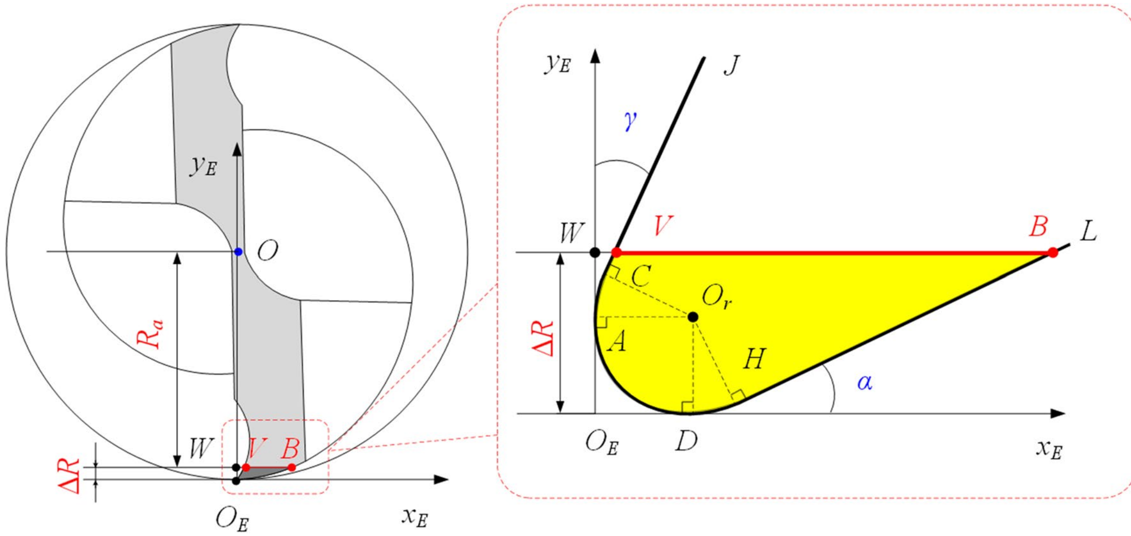


**Fig. 2** The relationship among the actual radius of the tool, tool flank wear, and tool edge radius

## 2.2 Modeling of the instantaneous uncut chip thickness

### 2.2.1 Actual tool radius

To accurately model the cutting force in the micro-end milling process, the actual tool radius model considering tool flank wear and tool edge radius will be given.

The cutting edge coordinate system $x_E O_E y_E$ is established at the bottom of the micro-end mill, as shown in Fig. 2. The straight line that passes through the center of the cutter and tangent to the arc of the cutting edge is the $y_E$ -axis, and the direction is from the tangent point to the cutter center. the $x_E$-axis is tangent to the arc of the cutting edge. The intersection $O_E$ of the $x_E$-axis and $y_E$ -axis is the origin. Figure 2 shows the relationship among the actual tool radius, tool flank wear, and tool edge radius. Line segment CJ, arc CAH, and line segment HL are the rake face, cutting edge arc, and flank face of the cutting edge respectively. Line segments VB, $O_E$W, and OW are the tool flank wear *VB*, shrinkage of tooth radius $\Delta R$, and actual radius of the tool $R_a$ respectively. Based on the modeling of the cutting part of the cutting edge, we can get the actual radius of the worn tool as

$$\begin{aligned} R_a &= R - \Delta R \\ &= R - \frac{VB + r(\cot\alpha - \csc\alpha - \tan\gamma - \sec\gamma)}{\cot\alpha - \tan\gamma} \end{aligned} \tag{6}$$

where $R$ is the radius of a fresh tool, $r$ is the tool edge radius, $\gamma$ and $a$ are the rake angle and clearance angle of the tool respectively.

### 2.2.2 Modeling of the instantaneous uncut chip thickness

Accurate IUCT modeling is essential for cutting force prediction in the micro-end milling process. The analysis and calculation of cutting edge trajectory is the key process of IUCT modeling. Under an ideal cutting situation, the cutting

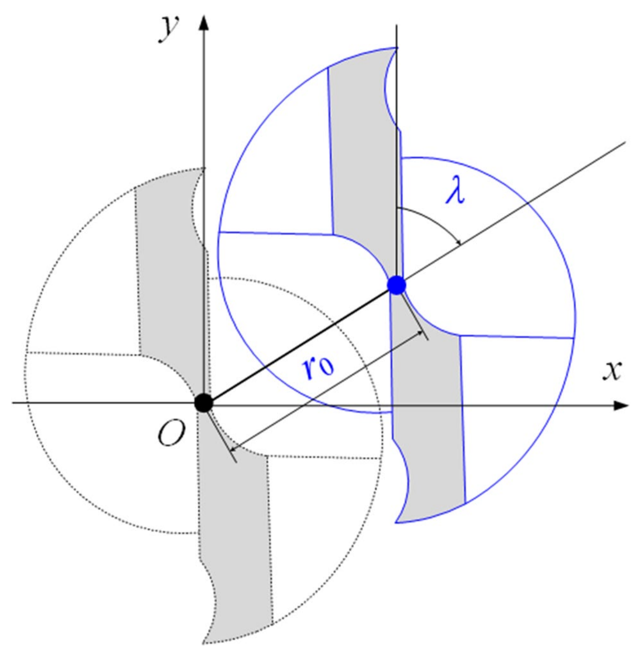


**Fig. 3** The geometry of tool runout

edge trajectory commonly referred to as trochoidal trajectories, is calculated by the path of the cutter location point, tool geometry, such as the number of cutter teeth and the tool radius, and the process parameters, such as the spindle speed and feed rate. But practically, the cutting edge trajectory will not only change with the cutter location point caused by tool runout but also with the reduction of the tool radius, that generally induced by tool wear accompanied by micro-cutting process. This section will elaborate on the calculation of the cutting edge trochoidal trajectories considering tool flank wear and tool runout, as well as further IUCT modeling.

The geometry of tool runout is shown in Fig. 3. The black dotted line and the blue solid line represent the ideal and actual tool positions, respectively. Tool runout distance $r_0$ is the distance between the ideal centerline and the actual centerline of the micro-end mill. Tool runout angle $\lambda$ is the angle from the $y$-axis direction to the offset direction. It is stipulated that the tool runout angle is positive, and vice versa.

Geometrically, the IUCT, as shown in Fig. 4 is the shortest distance between the current cutting edge trochoidal trajectory and workpiece surface generated by all previously passing cutting edges, in the direction perpendicular to the tangent of the current cutting edge trajectory, at the same cutter position angle in the micro-end milling process.

The IUCT is considered in different areas. In areas I and II, it is needed to consider trochoidal trajectories of the current cutting edge and all passing cutting edges in the previous cycle. In areas III and IV, it is needed to consider cutting edge trochoidal trajectories of the current and previous. The solid blue line and the dashed red line are the cutting edge trochoidal trajectories of the $i$ th and ($i$-1)th tooth considering tool flank wear and tool runout respectively. Points $P_i$ and $P_{i\text{-}j}$ are on the trochoidal trajectories of the $i$th and ($i$-$j$)th ($j = 1, 2, \ldots, N$) cutting edge at the time $t_i$ and $t_{i\text{-}j}$ respectively. $O_i$ and $O_{i\text{-}j}$ are the cutter centers of the points $P_i$ and $P_{i\text{-}j}$ respectively. The length of the line segment $P_iP_{i\text{-}j}$ is the IUCT.

Considering tool runout, the coordinates of the tool center $O_i$ and $O_{i\text{-}j}$ responding at the time $t_i$ and $t_{i\text{-}j}$ respectively, are given by

$$\begin{cases} x_{O_i} = \frac{ft_i}{60} + r_0 sin(\omega t_i + \lambda), \\ y_{O_i} = r_0 cos(\omega t_i + \lambda), \end{cases} \tag{7}$$

$$\begin{cases} x_{O_{i-j}} = \frac{ft_{i-j}}{60} + r_0 sin(\omega t_{i-j} + \lambda), \\ y_{O_{i-j}} = r_0 cos(\omega t_{i-j} + \lambda), \end{cases} \tag{8}$$

where $f$ is the feed rate(mm/min), and $f = nNf_z$, $f_z$ is the feed per tooth (μm/tooth).

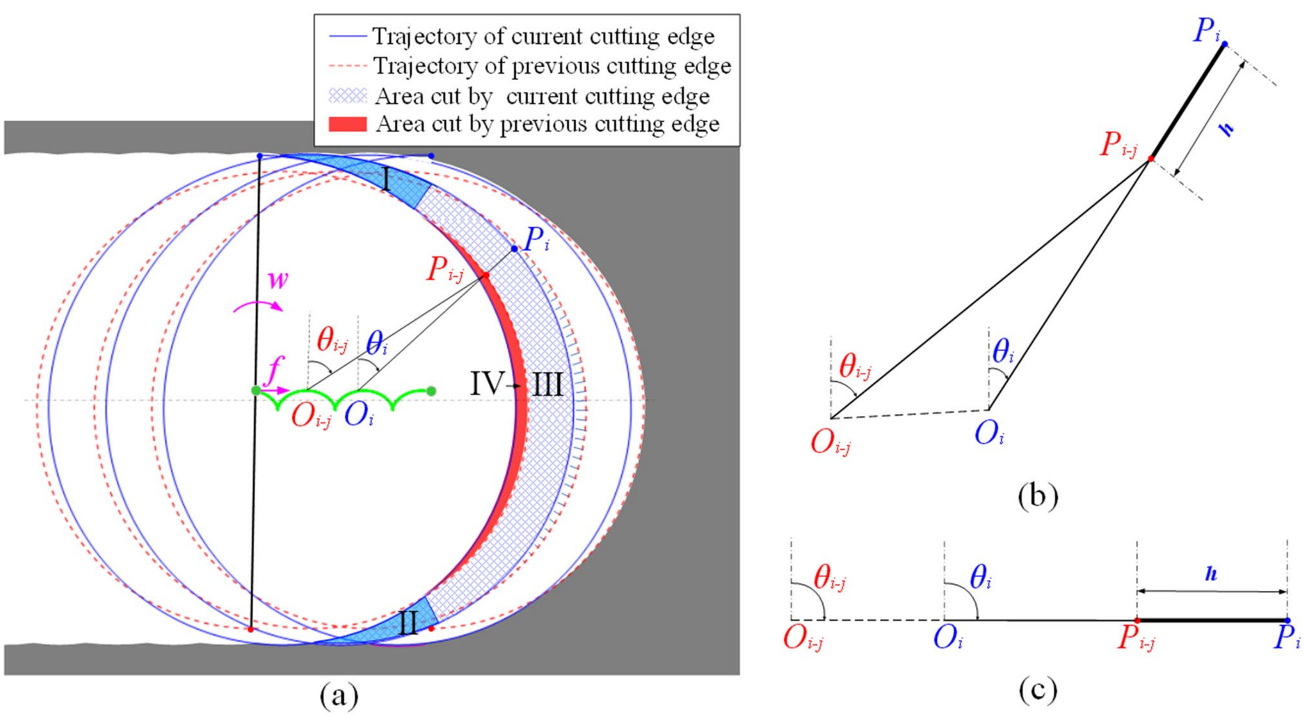


Fig. 4 IUCT for the micro-end mill of two teeth. (**a**) Cutting edge trochoidal trajectories considering tool flank wear, tool edge radius, and tool runout; (**b**) IUCT; (**c**) IUCT at a specific position

Point $P_i$ is on the current cutting edge at the position angle $\theta_i = \left(\omega t_i - \frac{2\pi i}{N} - \frac{z\tan\beta}{R_a}\right)$, whose coordinate is

$$\begin{cases} x_{P_i} = R_a sin\left(\omega t_i - \frac{2\pi i}{N} - \frac{z\tan\beta}{R_a}\right) + x_{O_i}, \\ y_{P_i} = R_a cos\left(\omega t_i - \frac{2\pi i}{N} - \frac{z\tan\beta}{R_a}\right) + y_{O_i}. \end{cases} \tag{9}$$

Similarly, the coordinate of the point $P_{i-j}$ on the trajectory of the previous tooth at the time $t_{i-j}$ is given by

$$\begin{cases} x_{P_{i-j}} = R_a sin\left(\omega t_{i-j} - \frac{2\pi(i-j)}{N} - \frac{z\tan\beta}{R_a}\right) + x_{O_{i-j}}, \\ y_{P_{i-j}} = R_a cos\left(\omega t_{i-j} - \frac{2\pi(i-j)}{N} - \frac{z\tan\beta}{R_a}\right) + y_{O_{i-j}}. \end{cases} \tag{10}$$

In Fig. 4(b), IUCT at position angle $\theta_i$ can be determined as follows:

$$\begin{aligned} h &= \left|P_iP_{i-j}\right| \\ &= \sqrt{\tan^2\theta_i + 1}\left|y_{P_i} - y_{P_{i-j}}\right| \\ &= \sqrt{\tan^2\theta_i + 1}\Big|R_a\cos\left(\omega t_i - \frac{2\pi i}{N} - \frac{z\tan\beta}{R_a}\right) + r_0\cos(\omega t_i + \lambda) \\ &-R_a\cos\left(\omega t_{i-j} - \frac{2\pi(i-j)}{N} - \frac{z\tan\beta}{R_a}\right) - r_0\cos(\omega t_{i-j} + \lambda)\Big|, \\ &(\theta_i \neq \tfrac{\pi}{2} + m\pi, m \in \mathbf{N}, \mathbf{N}\text{ is the natural numbers set}). \end{aligned} \tag{11}$$

In Eq. (11), $h$ is associated with variables $t_i$ and $t_{i-j}$. Usually, $t_{i-j}$ is calculated based on a given $t_i$. Consequently $t_{i-j}$ is the unique unknown variable in Eq. (11).

Since points $P_i$, $P_{i-j}$ and $O_i$ are on the same line, according to the geometric condition in Fig. 4(b), we can obtain:

$$\tan\left(\omega t_i - \frac{2\pi i}{N} - \frac{z\tan\beta}{R_a}\right) = \frac{x_{P_{i-j}} - x_{O_i}}{y_{P_{i-j}} - y_{O_i}} \tag{12}$$

By substituting Eqs.(7), (8), and (10) into Eq. (12), the equation of $t_{i-j}$ can be obtained as:

$$\begin{aligned} G(t_{i-j}) &= tan\left(\omega t_i - \frac{2\pi i}{N} - \frac{z\tan\beta}{R_a}\right)\Big[R_a\cos\left(\omega t_{i-j} - \frac{2\pi(i-j)}{N} - \frac{z\tan\beta}{R_a}\right) \\ &+r_0\cos(\omega t_{i-j} + \lambda) - r_0\cos(\omega t_i + \lambda)\Big]\text{-}R_a sin\left(\omega t_{i-j} - \frac{2\pi(i-j)}{N} - \frac{z\tan\beta}{R_a}\right) \\ &-\frac{ft_{i-j}}{60} - r_0 sin(\omega t_{i-j} + \lambda) + \frac{ft_i}{60} + r_0 sin(\omega t_i + \lambda) = 0. \end{aligned} \tag{13}$$

where $G(t_{i-j})$ is an auxiliary function for analysis conveniently.

Considering that Eq. (13) is a transcendental equation, the Newton iteration method is used for numerical solution. Considering the periodicity of the cutting process, the initial given value of iteration is

$$t_{(i-j)0} = t_i - \frac{60j}{nN}(n \in \mathbf{N}^*, \mathbf{N}^* \text{ is the positive integer set}).$$

Newton's iterative formula is

$$t_{(i-j)(k+1)} = t_{(i-j)k} - \frac{G(t_{(i-j)k})}{DG(t_{(i-j)k})}$$

where $DG(t_{(i-j)k})$ is the derivative function of function $G(t_{(i-j)k})$. And

$$\begin{aligned} DG(t_{i-j}) &= tan\left(\omega t_i - \frac{2\pi i}{N} - \frac{z\tan\beta}{R_a}\right)\Big[-\omega R_a\sin\left(\omega t_{i-j} - \frac{2\pi(i-j)}{N} - \frac{z\tan\beta}{R_a}\right) - \omega r_0\sin(\omega t_{i-j} + \lambda)\Big] \\ &-\omega R_a cos\left(\omega t_{i-j} - \frac{2\pi(i-j)}{N} - \frac{z\tan\beta}{R_a}\right) - \frac{f}{60} - \omega r_0 cos(\omega t_{i-j} + \lambda) = 0. \end{aligned}$$

When the solution $t_{i-j}$ of Eq. (11) is determined, the IUCT $h$ in Eq. (11) can be determined.

Especially, when $\theta_i = \frac{\pi}{2} + m\pi(m \in \mathbf{N}, \mathbf{N}$ is the natural numbers set), the line segment $O_iP_i$ is parallel to the $x$-axis, and points, $O_i$, $P_{i-j}$ and $P_i$ are on the same straight line that parallels the $x$-axis, as shown in Fig. 4(c). Now, IUCT is as follows:

$$\begin{aligned} h &= \left|P_iP_{i-j}\right| \\ &= \left|x_{P_i} - x_{P_{i-j}}\right| \\ &= \Big|R_a sin\left(\omega t_i - \frac{2\pi i}{N} - \frac{z\tan\beta}{R_a}\right) + \frac{ft_i}{60} + r_0 sin(\omega t_i + \lambda) \\ &-R_a sin\left(\omega t_{i-j} - \frac{2\pi(i-j)}{N} - \frac{z\tan\beta}{R_a}\right) - \frac{ft_{i-j}}{60} - r_0\sin(\omega t_{i-j} + \lambda)\Big|, \end{aligned} \tag{14}$$

and $t_{i-j} = t_i - \frac{2j\pi}{N\omega}$. Thus $h$ can be obtained.

## 3 Experimental verification and discussion

### 3.1 Experimental setup

Micro-end milling experiments were completed on the high-speed machining center MIKRON HSM600U, as shown in Fig. 5. The tool is a two-teeth cemented carbide micro-end mill. The diameter is 0.5 mm, the helix angle is 30°, the rake angle is 10°, the relief angle is 5°, and the tool edge radius is 2 μm. The workpiece material is AISI4340 alloy structural steel, and the workpiece size is 60 mm × 30 mm × 25 mm. Cutting forces were measured, and the figures of the worn tool were captured in the micro-milling process. The cutting forces were measured by a Kistler9119 three-component dynamometer, and the sampling frequency is 24 kHz. The industrial camera was used to capture the image of the worn tool by capturing the bottom of the micro-end mill.

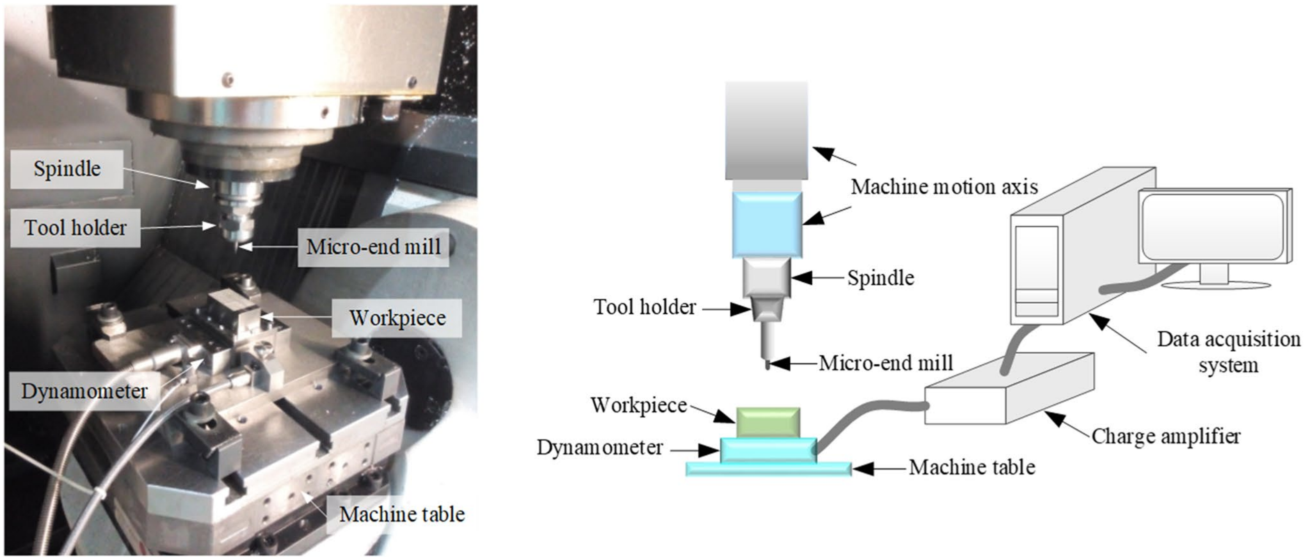


**Fig. 5** Experimental setup

**Table 1** Machining parameters of micro-milling tests

| Test No | Spindle speed $n$ (r/min) | Axial depth of cut $a_p$ (μm) | Feed per tooth $f_z$ (μm/tooth) |
|---|---|---|---|
| 1 | 18000 | 60 | 2 |
| 2 | 24000 | 80 | 6 |
| 3 | 30000 | 100 | 4 |

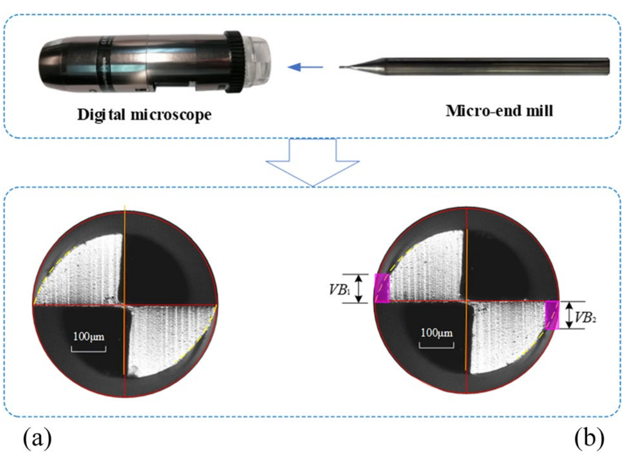


**Fig. 6** Image of tool flank wear in the micro-end milling. (**a**) A fresh tool; (**b**)After the 10th cutting

All the tests are full slot end milling, and the machining parameters are in Table 1. A fresh tool was used in each group test, and the tools are all the same brand, type, and batch. The images of the worn tool were captured per 60 mm of cutting length, and each test was cut 10 times. By using the measuring tool, the tool flank wear *VB* was got from the images of the worn tool. Figure 6 shows the images of the fresh tool and the tool flank wear image that is after the 10th cutting in test No.1. Due to the tool runout, the tool flank wear values of the two teeth are different. We take the average value $VB = (VB_1 + VB_2)/2$ as the tool flank wear.

## 3.2 Model verification and statistical analysis

### 3.2.1 Tool runout calibration

Tool runout parameters were the same in the 10 times cutting of each test with marking the tool holder. The tool runout parameter was calibrated as follows. First, by using the mean force method, we calibrated the cutting force coefficients in the $x$- and $y$-axis directions. Then, by traversing the tool runout parameters and calculating the IUCTs, we can get the corresponding simulated cutting forces. The tool runout parameter corresponds to the minimum square sum of the deviations of the simulated forces and the measured forces.

The calibrated tool runout results are shown in Table 2.

**Table 2** Results of tool runout

| Test No | $r_0$ (μm) | $\lambda$ (deg) |
|---|---|---|
| 1 | 1.535 | 75 |
| 2 | 1.805 | 61 |
| 3 | 0.336 | 85 |

#### 3.2.2 Cutting force coefficients calibration

The increased forces caused by tool wear are present in the form of increments in each cutting force coefficient in the cutting force model. Given this, it is assumed that the increments in the cutting force coefficients caused by tool flank wear are in the form of a quadratic polynomial over *VB*. Then the cutting force coefficients considering tool flank wear are as follows:

$$\begin{cases} K_{tc} = k_{tc} + \alpha_{tc} VB^2 + b_{tc} VB + c_{tc}, \\ K_{rc} = k_{rc} + \alpha_{rc} VB^2 + b_{rc} VB + c_{rc}, \\ K_{ac} = k_{ac} + \alpha_{ac} VB^2 + b_{ac} VB + c_{ac}, \end{cases}$$

where $K_{tc}$, $K_{rc}$, and $K_{ac}$ are the cutting force coefficients in tangential, radial, and axial directions of a fresh tool, respectively, $a_{tc}$, $b_{tc}$, $c_{tc}$, $a_{rc}$, $b_{rc}$, $c_{rc}$, $a_{ac}$, $b_{ac}$, and $c_{ac}$ are constant parameters determined by fitting.

The exact values of the cutting force coefficients (N/mm$^2$) for Test No.1 are

$$\begin{cases} K_{tc} = 20.64VB^2 - 1545VB + 46700 \\ K_{rc} = 9.699VB^2 - 803.8VB + 29620 \\ K_{ac} = 1.037VB^2 - 89.7VB + 2051 \end{cases}$$

The exact values of the cutting force coefficients (N/mm$^2$) for Test No.2 are

$$\begin{cases} K_{tc} = 1.096VB^2 + 15.37VB + 6300 \\ K_{rc} = 0.2532VB^2 + 65.43VB + 3664 \\ K_{ac} = 0.1602VB^2 - 8.963VB + 189.3 \end{cases}$$

The exact values of the cutting force coefficients (N/mm$^2$) for Test No.3 are

$$\begin{cases} K_{tc} = 2.83VB^2 - 194.2VB + 19500 \\ K_{rc} = 2.166VB^2 - 146.8.8VB + 14970 \\ K_{ac} = 0.3711VB^2 - 27.69VB + 601 \end{cases}$$

#### 3.2.3 Statistic analysis

Three indicators are used to evaluate the validity of the presented cutting force model.

a) Peak error *Ep*:

$$E_p = \left| \frac{|F_{si}|_{\max} - |F_{mi}|_{\max}}{|F_{mi}|_{\max}} \right| \times 100\%,$$

where $F_{mi}$ and $F_{si}$ ($i = 1,2, \ldots, l$, where $l$ is the number of sampling points) are the measured forces and simulated forces respectively. The peak value of cutting forces can directly reflect the machining state that the largest tool load in the whole cutting process. It affects the tool life and the quality of the processed products, and it is an important index to measure the machining state.

b) Median absolute error *MedianAE*:

$$MedianAE(F_m, F_s) = median(|F_{m1} - F_{s1}|, |F_{m2} - F_{s2}|, \cdots\cdots, |F_{mn} - F_{sl}|).$$

It refers to the median of the absolute error between the predicted forces and the measured forces, which is robust to the outliers of the target variable and can weaken the influence of outliers.

c) Normalized root mean square error *NRMSE*:

$$NRMSE = \frac{RMSE}{F_{m\max} - F_{m\min}},$$

where $F_{m\max}$ and $F_{m\max}$ are the maximum and minimum of the measured forces respectively, *RMSE* is the root mean square error. *NRMSE* is an effective method to evaluate the fitted data, which overcomes the scale dependence and simplifies the comparison between models of different scales or data sets.

To highlight the effect of tool flank wear on the cutting force in the micro-end milling process, we take the results of the 10th milling of each group test as an example, and the results are shown in Figs. 7, 8, and 9.

The peak error *Ep* of the predicted force in the three directions of the 3 group tests is shown in Fig. 7. The peak

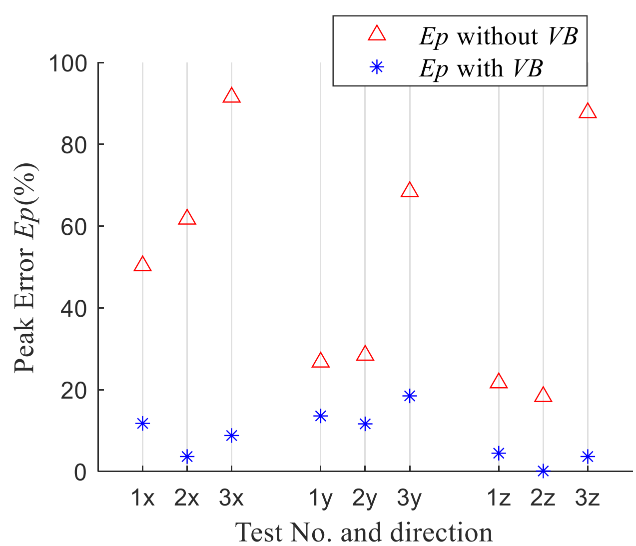


**Fig. 7** The peak error

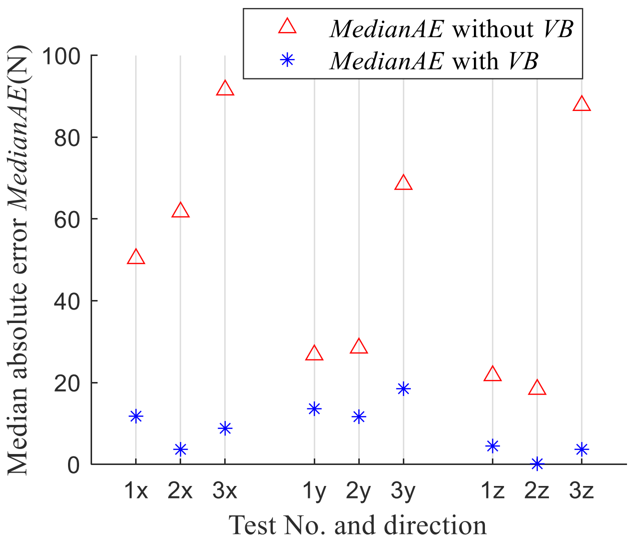


**Fig. 8** Median absolute error

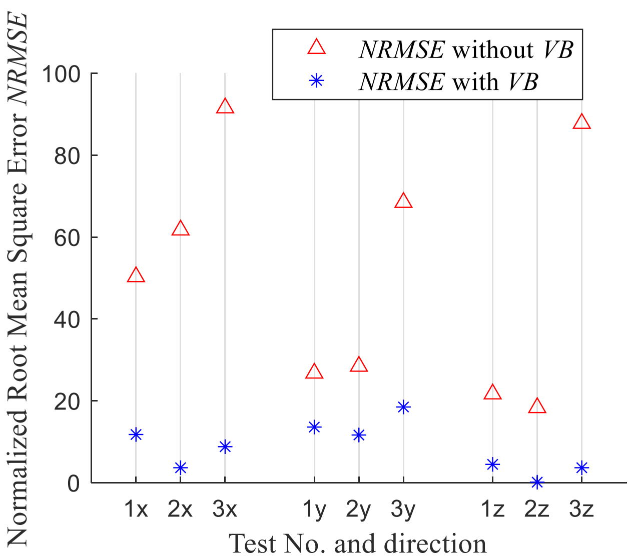


**Fig. 9** Normalized root mean square error

errors in the *x*-, *y*- and *z*-axis directions are less than 13.59%, 11.65%, and 18.49% respectively. It indicates that the proposed model is correct. Compared to ignoring the tool flank wear, the peak error values in the three directions decreased by more than 13.16%, 16.77%, and 49.95% respectively. This shows that the influence of tool flank wear on cutting force cannot be ignored in the whole cutting process.

The Median absolute error *MedianAE* of the predicted forces in three directions for the 3 group tests is shown in Fig. 8. The *MedianAE* in the *x*-, *y*- and *z*-axis directions are less than 0.83N, 0.80N, and 0.59N respectively. Compared with that not considering tool flank wear, the *MedianAE* in the three directions are reduced by more than 0.32N, 0.22N, and 0.25N respectively.

The Normalized root mean square error *NRMSE* of the simulated forces in three directions for 3 group tests is shown in Fig. 9. The *NRMSE* in the *x* -, *y*—and *z*-axis directions are less than 0.14, 0.27, and 0.43 respectively. Compared with that not including tool flank wear, the *NRMSE* in the three directions are reduced by more than 0.08, 0.13, and 0.17 respectively.

Figure 7, 8, and 9 show that compared to that ignoring tool flank wear, the deviation of the simulated forces and the corresponding measured forces are smaller when tool flank wear is not considered from different aspects. This indicates that the proposed cutting force model is effective, and it is essential to include tool flank wear in the cutting force modeling.

## 3.3 Influence of tool flank wear

In all three groups of tests, the influences of tool flank wear on the IUCT and the cutting forces are consistent. Therefore, it is advisable to take the test No.1 as a case for detailed analysis. Test No.1 is discussed below to explore the influence of tool flank wear.

### 3.3.1 Influence of tool flank wear on the IUCT

Due to the influence of the helix angle of the cutting edge, the IUCT varies slightly at different cutting depths, but the overall trend is consistent. Taking the element at 1/2 axial cutting depth as an example, the effect of tool flank wear on the IUCT is studied below, as shown in

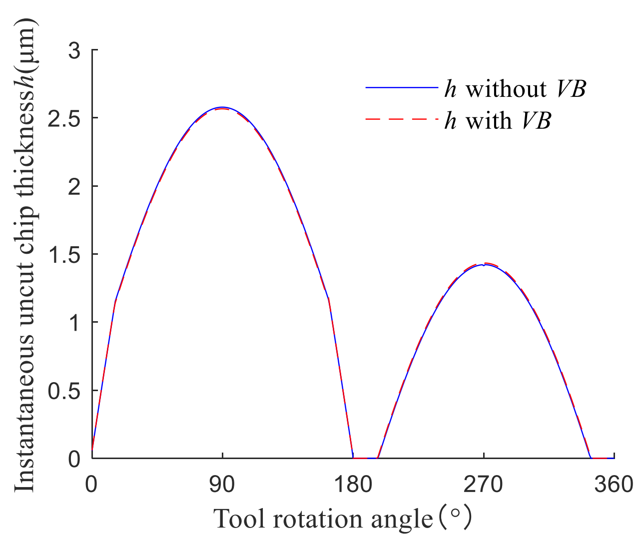


**Fig. 10** IUCT without considering tool flank wear and the 10th milling in test No.1

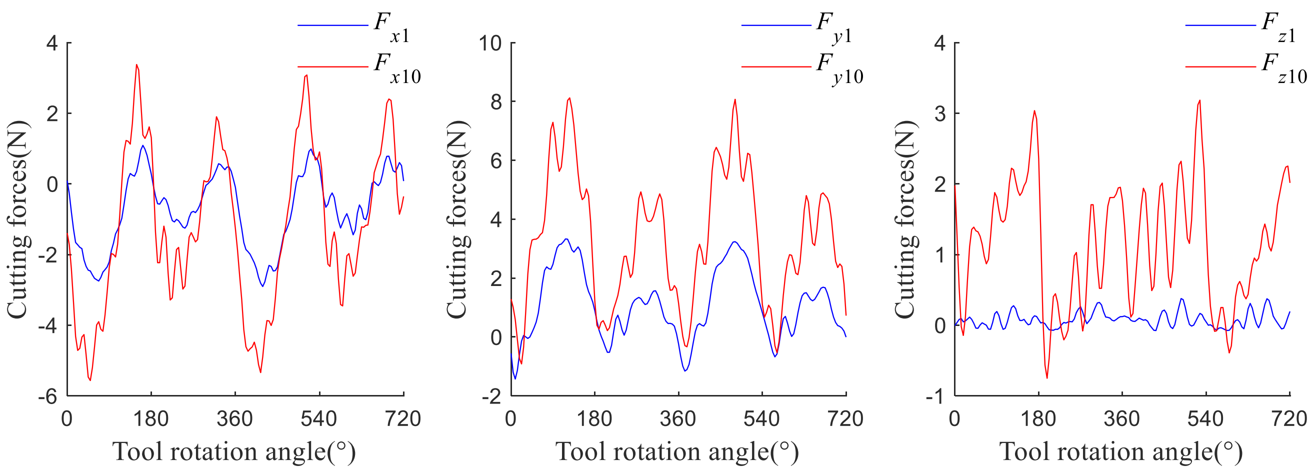


**Fig. 11** Measured cutting forces of the 1st and 10th milling in Test No. 1

Fig. 10. It shows the IUCT neglecting tool flank wear and the 10th cutting corresponding to $VB = 76.2$ μm in test No.1. The prediction results show that the tool flank wear has a slight effect on the IUCT. The tool flank wear leads to a decrease of 0.47% in the maximum IUCT of the first tooth and an increase of 0.84% in the maximum IUCT of the second tooth, even if the effect is not significant. Due to the fixed cutting parameters, the total cutting amount remains unchanged, so within a certain range, the change of IUCT is relatively small due to the reduction of tool radius caused by the tool flank wear. The unsmooth of IUCT curve is near tool rotation angles of 16° and 163°, which are corresponding to the transition area from area I to area III and the transition area from area III to area II respectively in Fig. 3. These results are attributed to the consideration of the trochoidal trajectories of current cutting edge and all passing cutting edges in the previous cycle.

#### 3.3.2 Influence of tool flank wear on the cutting forces

The measured cutting forces of the 1st cutting and the 10th cutting in test No.1 are shown in Fig. 11. Results show that tool flank wear does not affect the waveform of cutting force. The amplitudes of cutting forces in the *x*-, *y*-, and *z*-axis directions increase by 102%, 144%, and 842% respectively of the 10th cutting, compared with those of the 1st cutting. This shows that the influence of tool flank wear on the cutting forces in the three directions cannot be ignored throughout the entire cutting process. In particular, the effect on the *z*-axis force is the largest, which is due to the increase in axial cutting thickness caused by the axial wear of the bottom of the tool.

The cutting forces of the 1st and 10th cutting in test No.1 are shown in Fig. 12. Figure 12(a) and (b) are the comparison between the predicted forces and the measured forces of the 1st cutting. Results show that the predicted cutting forces agree well with the measured cutting forces whether to consider the tool flank wear. This is because the small cutting length leads to a small amount of tool flank wear, whose impact on the cutting forces is not significant. Figure 12(c) -(d) show the comparison between the predicted forces and the measured forces of the 10th cutting. The results show that the predicted cutting forces of the proposed model considering tool flank wear are consistent with the experimental forces respectively, and the deviation of the predicted forces is significant when the flank wear is not considered. It is explained that the influence of tool flank wear on cutting forces cannot be ignored in the whole cutting process.

## 4 Conclusions

This paper focuses on the accurate prediction of cutting force in the micro-end milling process, the modeling of IUCT and cutting force are performed by considering tool flank wear, tool edge radius, and tool runout comprehensively. The proposed model is verified by micro-end milling experiments and the experimental results are statistically analyzed. The following conclusions are drawn.

By evaluating the peak error *Ep* of cutting force in the micro-end milling process, it is found that the predicted forces are in good agreement with the experimental results, which verifies that the proposed model is effective.

By evaluating the three statistical indicators including peak absolute error *Ep*, median absolute error *MedianAE* and normalized root mean square error *NRMSE*, it is found that the influence of tool flank wear on cutting forces cannot be ignored during the whole cutting process.

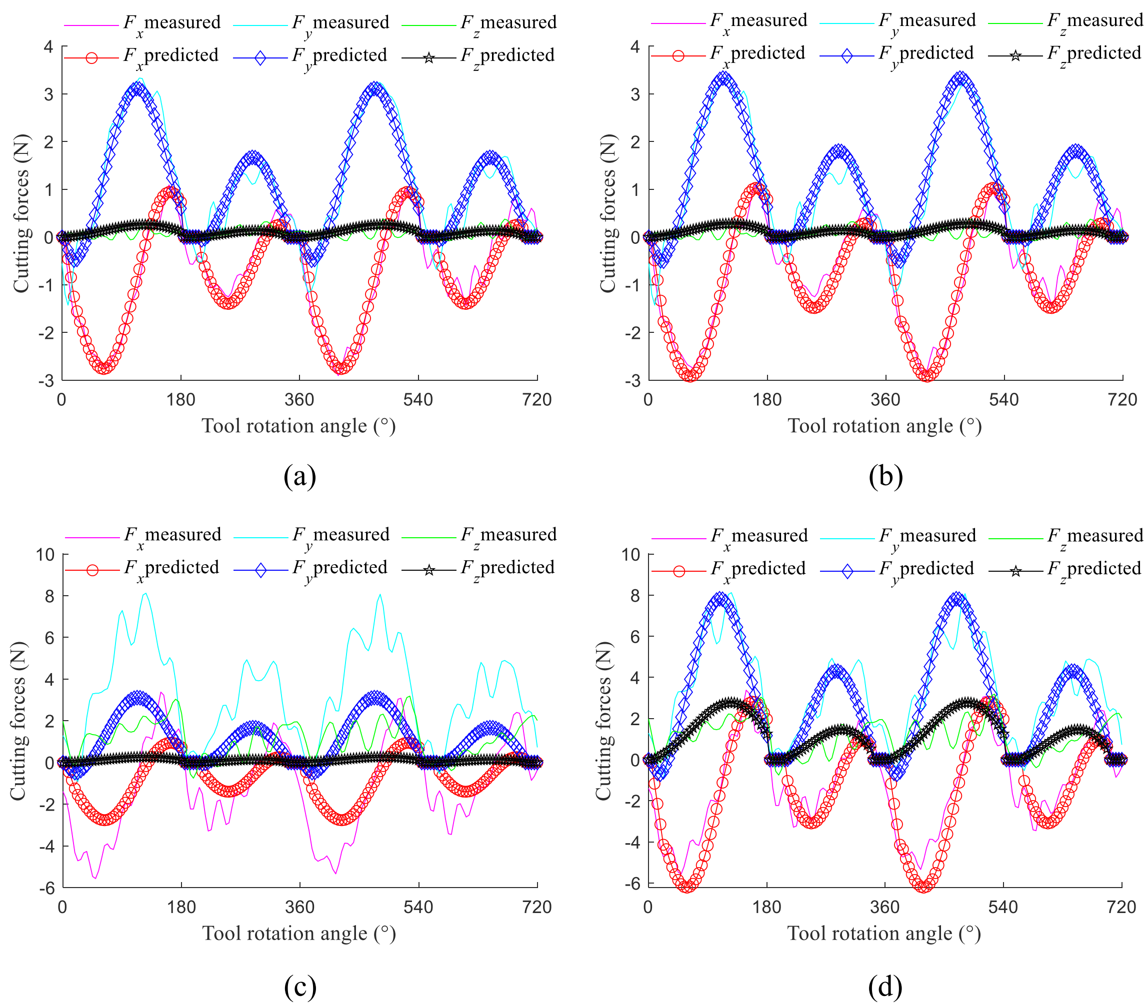


**Fig. 12** The 1st cutting and 10th cutting in test No.1. (**a**)The 1st cutting without considering tool flank wear; (**b**) The 1st cutting considering tool flank wear; (**c**) The 10th cutting without considering tool flank wear; (**d**) The 10th cutting considering tool flank wear

Through a case study, it is found that the impact of tool flank wear on the 3-direction cutting forces cannot be ignored throughout the entire cutting process, and the influence on the axial force is the most significant.

By predicting the IUCT, it is found that the decrease of tool radius caused by tool flank wear within a certain range has a relatively small effect on the IUCT. The proposed model of cutting force model can be extended to 3D modeling to establish a more general micro-milling force model.

**Author contributions** Xianyin Duan, Kunpeng Zhu, and Shuaishuai Gao proposed the method of the paper. Kunpeng Zhu and Yu Zhang provided the experimental settings and data. Shuaishuai Gao and Xianyin Duan wrote the first draft of the article and completed the programming prediction and experimental data analysis. Shuaishuai Gao completed the modification and polish of the whole manuscript and drawing of all the figures and tables. Xianyin Duan, Kunpeng Zhu and Yu Zhang made many constructive suggestions for the modeling, experiments and the writing of the whole paper. All authors have read and agreed to the published.

**Funding** This research was supported by the National Natural Science Foundation of China (No. 51605346). Key research and development program of Hubei Province (2022BAA059).

**Data availability** The measuring data in our paper are available from the corresponding author by request, and other related materials can also be obtained from the corresponding author.

**Code availability** The code for cutting force model during the study is available from the corresponding author by request.

## Declarations

**Ethics approval** Not applicable.

**Consent to participate** All authors and facilitators have certified their participation in this work.

**Consent for publication** All authors certify that they consent to publish the article. The article is the author's original work and has not been published in advance or considered for publication elsewhere.

**Conflicts of interest** The authors have no relevant financial or non-financial interests to disclose. The authors have no conflicts of interest to declare that are relevant to the content of this article. All authors certify that they have no affiliations with or involvement in any organization or entity with any financial interest or non-financial interest in the subject matter or materials discussed in this manuscript.

## References


1. Anand RS, Patra K (2014) Modeling and simulation of mechanical micro-machining-a review. Mach Sci Technol 18(3):323–347
2. Davim JP (2014) Modern mechanical engineering: Research, development and education. Springer Science & Business Media, London
3. Balázs BZ, Geier N, Takács M, Davim JP (2021) A review on micro-milling: recent advances and future trends. Int J Adv Manuf Technol 112(3):655–684
4. Chen N, Li HN, Wu J, Wu JM, Li ZJ, Li L, Liu GY, He N (2020) Advances in micro-milling: from tool fabrication to process outcomes. Int J Mach Tools Manuf 160:103670
5. Altintas Y (2000) Manufacturing Automation: Metal Cutting Mechanics, Machine Tool Vibrations, and CNC Design. Cambridge University Press, UK
6. Bao WY, Tansel IN (2000) Modeling micro-end milling operations. Part I: analytic cutting force model. Int J Mach Tools Manuf 40(15):2155–2173
7. Zhang XW, Yu TB, Dai YX, Qu S, Zhao J (2020) Energy consumption considering tool wear and optimization of cutting parameters in micro-milling process. Int J Mech Sci 178:105628
8. Zhu KP, Li G (2021) Theoretical modeling and experimental study of micro-milling force based on tool wear mapping. J Mech Eng 19:246–259
9. Bao WY, Tansel IN (2000) Modeling micro-end milling operations. Part II: tool runout. Int J Mach Tools Manuf 40(15):2175–2192
10. Vogler MP, DeVor RE, Kapoor SG (2005) On the modeling and analysis of machining performance in Micro-End milling, Part II: Cutting Force Prediction. J Manuf Sci Eng 126:695–705
11. Rodríguez P, Labarga JE (2013) A new model for the prediction of cutting forces in micro-end-milling operations. J Mater Process Tech 213(2):261–268
12. Zhang XW, Ehmann KF, Yu TB, Wang WS (2016) Cutting forces in micro-end milling processes. Int J Mach Tools Manuf 107:21–40
13. Li K, Zhu K, Mei T (2016) A generic instantaneous undeformed chip thickness model for the cutting force modeling in micromilling. Int J Mach Tool Manuf 105:23–31
14. Moges TM, Desai KA, Rao PVM (2018) Modeling of cutting force, tool deflection, and surface error in micro-milling operation. Int J Adv Manuf Technol 98:2865–2881
15. Wojciechowski S, Matuszak M, Powałka B, Madajewski M, Maruda RW, Krolczyk GM (2019) Prediction of cutting forces during micro end milling considering chip thickness accumulation. Int J Mach Tools Manuf 147:103466
16. Wan M, Wen DY, Ma YC, Zhang WH (2019) On material separation and cutting force prediction in micro-milling through involving the effect of dead metal zone. Int J Mach Tools Manuf 146:103452
17. Moges TM, Desai KA, Rao PVM (2016) Improved process geometry model with cutter runout and elastic recovery in micro-end milling. Procedia Manuf 5:478–494
18. Yuan YJ, Jing XB, Ehmann KF, Cao J, Li HZ, Zhang DW (2018) Modeling of cutting forces in micro end-milling. J Manuf Process 31:844–858
19. Jing XB, Lv R, Chen Y, Tian Y, Li H (2020) Modelling and experimental analysis of the effects of runout, minimum chip thickness and elastic recovery on the cutting force in micro-end milling. Int J Mech Sci 176:105540
20. Jing XB, Lv R, Song B, Xu J, Jaffery S (2021) A novel run-out model based on spatial tool position for micro-milling force prediction. J Manuf Process 68:739–749
21. Wan M, Wen DY, Zhang WH, Yang Y (2023) Prediction of cutting forces in flexible micro milling processes by considering the change of instantaneous cutting direction. J Manuf Process 90:180–195
22 Bao WY, Tansel IN (2000) Modeling micro-end milling operations. Part III: influence of tool wear. Int J Mach Tools Manuf 40(15):2193–2211
23. Li G, Li S, Zhu K (2020) Micro-milling force modeling with tool wear and runout effect by spatial analytic geometry. Int J Adv Manuf Technol 107(9):631–343
24. Liu T, Liu Y, Zhang K (2022) An improved cutting force model in micro-milling considering the comprehensive effect of tool runout, size effect and tool wear. Int J Adv Manuf Technol 120:659–668
25. Gao S, Duan X, Zhu K, Zhang Y (1805) Generic cutting force modeling with comprehensively considering tool edge radius, tool flank wear and tool runout in micro-end milling. Micromachines 2022:13




**Prime novelty statement** This manuscript titled of ***Influence of tool flank wear with considering tool edge radius on instantaneous uncut chip thickness and cutting force in micro-end milling*** is original, it is not submitted to else journals simultaneously, and all authors agree to submit it to The International Journal of Advanced Manufacturing Technology. Moreover, this is a preliminary, novel research paper.